A Reactive Power Boosting Strategy for BESS-STATCOMs

Joseph Kiran Banda, *Member, IEEE*, Lucas Savoi Araujo, Salvatore D'Arco, Tor-Eivind Moen, and Elisabetta Tedeschi, *Senior Member, IEEE*

***Abstract*—The integration of conventional STATCOMs with a battery energy storage system (BESS-STATCOM) has been gaining popularity recently. A BESS-STATCOM is interfaced to the grid via a power conversion system (PCS). This PCS is often a single-stage dc–ac converter directly connected to the BESS without an intermediate dc–dc converter to reduce costs and size. In this configuration, BESS's voltage drops associated with a lower state of charge (SoC) can reduce the capabilities of the BESS-STATCOM to inject reactive power. This article introduces a control strategy to boost the reactive power capabilities of a BESS-STATCOM with a single-stage PCS. The proposed strategy disconnects the battery pack from the PCS and charges the dc link capacitor to its full rated voltage from the grid. The transition into the boost mode and vice versa is seamlessly performed at zero battery pack's current, eliminating the need for a dc circuit breaker. The effectiveness of the proposed control strategy is validated through a Matlab/Simulink simulation using a 5 MVA BESS-STATCOM, followed by an experimental validation using a 32.5 kVA scaled-down PCS. The results show that when the battery pack's SoC is at 20% , the proposed strategy increases the reactive power capability approximately threefold compared to the scenario without the strategy.**

***Index Terms*—BESS-STATCOM, battery fed converters, grid support services, grid-scale energy storage, power conversion systems (PCSs).**

I. Introduction

CONVENTIONAL static synchronous compensators (STATCOMs) are typically connected to the electrical grid to regulate voltage and provide dynamic reactive power control [1]. Recently, these devices are being tasked with supplying, not just reactive power, but also active power for services like fast frequency response or peak-shaving [2]. Consequently, an energy source, such as battery energy storage systems (BESS), must be integrated into STATCOMs to form what can be referred to as BESS-STATCOMs [3].

BESS-STATCOMs are grid-connected through a power conversion system (PCS), which typically consists of a single-stage converter [4], [5]. This means that the BESS is connected without an intermediate dc/dc converter that can fix the output voltage. This setup is commonly chosen for industrial off-the-shelf products [6], due to lower initial costs [7]. Single-stage PCSs are also more compact, which is especially important in space-constrained applications.

In BESS-STATCOMs, when the battery is discharged, it makes sense to prioritize ancillary services related to reactive power provision rather than active power because the active power availability depends on the BESS state of charge (SoC).

Nonetheless, the provision of reactive power also faces challenges due to the reduced BESS SoC in single-stage PCS setups. This issue arises because a converter's capability to supply reactive power is predominantly related to the dc bus and grid voltage levels. Hence, when the SoC of a BESS-STATCOM with a single-stage PCS is low, the available dc bus voltage for the PCS is reduced, and consequently, its reactive power supply capability should be limited, as the PCS would otherwise reach overmodulation. This issue is the prime motivation of this article.

In recent years, substantial efforts have been dedicated to refining the control of BESS-STATCOMs to provide both active and reactive power, aiming to address power quality issues in electrical grids. In [8], it is shown that integrating a BESS-STATCOM into a power system can provide system damping and improved transient power angle stability and voltage and frequency regulation. In [9] and [10], a single-stage PCS for BESS-STATCOM provides active and reactive power and regulates the grid frequency and voltage.

In [11], a two-stage PCS is used as a BESS-STATCOM for a motor starting application, curtailing the BESS active power momentarily and providing a large amount of reactive power when there is a voltage disturbance. Notably, the author's proposal is to use the entire rated capability of the PCS to provide only reactive power, rather than using the remaining capability after active power provision. A two-stage PCS for BESS-STATCOM is also used in [12] to provide simultaneous active and reactive power as a function of frequency and voltage variations, respectively. In addition, a reactive power prioritization is proposed whenever voltage regulation is more critical than frequency support.

In [13], fluctuations in voltage and frequency within an isolated marine grid are smoothed through the utilization of

Received 13 June 2024; revised 16 September 2024, 24 November 2024, and 30 January 2025; accepted 23 February 2025. Date of publication 26 February 2025; date of current version 23 October 2025. This work was supported by the Program PETROMAKS2 of the Research Council of Norway through the project "Smart Platform," under Grant 308735. *(Corresponding author: Joseph Kiran Banda.)*

Joseph Kiran Banda and Lucas Savoi Araujo are with the Department of Electric Energy, Norwegian University of Science and Technology, 7034 Trondheim, Norway (e-mail: joseph.kiran.banda@ntnu.no).

Salvatore D'Arco is with the SINTEF Energy Research, 7034 Trondheim, Norway.

Tor-Eivind Moen is with the ABB, 0303 Oslo, Norway.

Elisabetta Tedeschi is with the Department of Electric Energy, Norwegian University of Science and Technology, 7034 Trondheim, Norway, and also with the Department of Industrial Engineering, University of Trento, 38122 Trento, Italy.

Digital Object Identifier 10.1109/JESTIE.2025.3545888

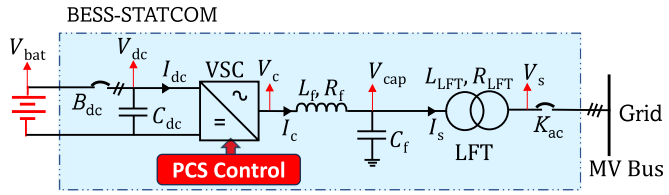

Fig. 1. Single line diagram of single stage BESS-STATCOM.

a grid-supporting BESS embedded with a data-driven control when providing active and reactive power. In [14] and [15], it is shown that the PQ capability curve of a single-stage PCS changes as function of the dc bus voltage and grid voltage values, and optimization methods are proposed to provide frequency control and voltage support from BESS. The dc bus voltage variation of an energy storage integrated statcom (ES-STATCOM) due to its connected energy system is also evaluated in [16], and a cost-effective interface converter is proposed to regulate that voltage fluctuation.

The referenced research papers highlight a growing trend towards utilizing BESS-STATCOMs for grid support functions. Yet, either these studies frequently overlook the influence of the battery discharge and its associated voltage on the variability of the PCS reactive power capability, or they implement a double-stage PCS arrangement to overcome it [17]. Other common approaches to dealing with this issue are oversizing the BESS-STATCOM PCS converter, or changing the tap changer position of the BESS-STATCOM connection transformer. While oversizing a converter and using a double-stage arrangement can offer extra reactive power support, these approaches involve tradeoffs in terms of cost, efficiency, space, and complexity. In addition, transformers typically have a limited number of taps, so changing the tap might offer a discrete set of options for voltage adjustment.

This article proposes a novel strategy that boosts the reactive power capabilities in BESS-STATCOMs with a single-stage PCS without any converter-hardware upgrade, thus, addressing a gap in the literature. The contributions of this article can be summarized as follows.

1) Proposing a novel control method to achieve reactive power boost from a BESS-STATCOM utilizing dynamic power capability curves.
2) Proving that the reactive power boost effectively raises the BESS-STATCOM's reactive power capability to match that of a BESS-STATCOM with a fully charged battery pack.
3) Ensuring seamless transitions from normal mode to boost mode and vice versa at zero battery pack current, thus eliminating the need for a dc circuit breaker.

II. System Description and Theoretical Analysis of BESS-STATCOM

A simplified single-line diagram of a BESS-STATCOM is shown in Fig. 1 integrated into the power system at the medium voltage (MV) bus. The BESS-STATCOM mainly comprises a centralized battery pack, a single-stage dc–ac PCS (or multiple of them in parallel depending on the requirement), and a control system. A 2-level voltage source converter (VSC) with filter reactor L_f, filter capacitor C_f, and a LV/MV line frequency transformer (LFT) realizing an LCL filter forms the power circuit of the PCS. A dc contactor (B_{dc},) connects the VSC to the battery pack, whereas an ac contactor (K_{ac},) connects LFT to the grid. The battery pack is realized by combining multiple cells in series and parallel to produce a dc bus and the desired energy.

A. Active and Reactive Power Capability of BESS-STATCOM

The primary component responsible for utilizing the BESS as a reactive power source is the PCS. The magnitude of the maximum power flow is determined by the ac and dc voltages at the terminals of the conversion equipment, as well as the peak voltage and current ratings of the semiconductor devices. To better understand how the involved quantities limit the active and reactive power flow through the power conversion equipment, a mathematical derivation is presented to evaluate the active and reactive power capabilities of the VSC in Fig. 1 at the point of connection to the grid

$$
\begin{aligned}
&Z_{\mathrm{LFT}} = R_{\mathrm{LFT}} + j\omega_{\mathrm{n}} L_{\mathrm{LFT}}; \quad Z_{\mathrm{f}} = R_{\mathrm{f}} + j\omega_{\mathrm{n}} L_{\mathrm{f}} \\
&X_{\mathrm{Cf}} = \frac{1}{\omega_{\mathrm{n}} C_{\mathrm{f}}} \\
&v_{\mathrm{capdq}} = R_{\mathrm{LFT}} i_{\mathrm{sdq}} + L_{\mathrm{LFT}} \frac{d}{dt} i_{\mathrm{sdq}} + j\omega_{\mathrm{n}} L_{\mathrm{LFT}} i_{\mathrm{sdq}} + v_{\mathrm{sdq}} \\
&v_{\mathrm{cdq}} = R_{\mathrm{f}} i_{\mathrm{cdq}} + L_{\mathrm{f}} \frac{d}{dt} i_{\mathrm{cdq}} + j\omega_{\mathrm{n}} L_{\mathrm{f}} i_{\mathrm{cdq}} + v_{\mathrm{capdq}} \\
&i_{\mathrm{cdq}} = i_{\mathrm{sdq}} + C_{\mathrm{f}} \frac{d}{dt} v_{\mathrm{capdq}} + j\omega_{\mathrm{n}} C_{\mathrm{f}} v_{\mathrm{capdq}}.
\end{aligned} \tag{1}
$$

The voltages and currents in (1) are shown in a rotating reference frame [18]. The angle for transforming variables from the stationary reference frame to the rotating reference frame (dq) is obtained from a phase-locked loop (PLL) such that the vector aligned to the direct axis is in phase with the measured capacitor voltage. Z_{LFT} and Z_{f} are the complex leakage impedances of the LFT and converter reactor, respectively. L_{LFT} and R_{LFT} are leakage inductance and leakage resistance of the LFT referred to the LV side. The variables v_{capdq}, v_{cdq}, i_{cdq}, v_{sdq}, and i_{sdq} denote the instantaneous fundamental rotating vectors of the filter capacitor voltage, VSC voltage, VSC current, source voltage (referred to LV side), and source current, respectively, while ω_{n} is the fundamental angular frequency. For steady-state analysis, derivative terms are omitted from (1) to derive a generic form of the source current for a VSC with an *LCL* filter, as shown in (5). The mathematical steps leading to this result are detailed in (2), (3), and (4)

$$
v_{\mathrm{cdq}} = i_{\mathrm{cdq}} Z_{\mathrm{f}} + i_{\mathrm{sdq}} Z_{\mathrm{LFT}} + v_{\mathrm{sdq}} \tag{2}
$$

$$
(v_{\mathrm{cdq}} - v_{\mathrm{sdq}}) = i_{\mathrm{sdq}} Z_{\mathrm{LFT}} + Z_{\mathrm{f}} \left(i_{\mathrm{sdq}} + j \frac{v_{\mathrm{capdq}}}{X_{\mathrm{Cf}}} \right) \tag{3}
$$

$$(v_{\text{cdq}} - v_{\text{sdq}}) = i_{\text{sdq}} Z_{\text{LFT}} + Z_{\text{f}} \left(i_{\text{sdq}} + j \left(\frac{Z_{\text{LFT}} i_{\text{sdq}} + v_{\text{sdq}}}{X_{\text{Cf}}} \right) \right) \tag{4}$$

$$i_{\text{sdq}} = \frac{v_{\text{cdq}} - v_{\text{sdq}} \left(1 + j \frac{Z_{\text{f}}}{X_{\text{Cf}}}\right)}{Z_{\text{LFT}} + Z_{\text{f}} + j \frac{Z_{\text{LFT}} Z_{\text{f}}}{X_{\text{Cf}}}}. \tag{5}$$

Once the source current i_{sdq} is computed, the three-phase instantaneous active (P_{pcs}) and reactive (Q_{pcs}) powers of the BESS-STATCOM at the point of connection to the grid can be calculated as

$$P_{\text{pcs}} = 1.5 \cdot \text{Real} \left(v_{\text{sdq}} \cdot i^*_{\text{sdq}} \right) \tag{6}$$

$$Q_{\text{pcs}} = 1.5 \cdot \text{Imag} \left(v_{\text{sdq}} \cdot i^*_{\text{sdq}} \right)$$

$$\text{subject to:} \quad |v_{\text{cdq}}| \leq (1.15 \cdot 0.5 \cdot V_{\text{dc}})$$

$$|i_{\text{cdq}}| \leq (I_{\text{base}} \cdot \sqrt{2}) \tag{7}$$

where i^*_{sdq} is the complex conjugate of i_{sdq}. Notably, both P_{pcs} and Q_{pcs} are constrained by two limits established during the design phase of the PCS.

1) *PCS voltage limit:* For a modulation index (MI) of 1.0 per unit, the peak value of the converter voltage ($|v_{\text{cdq}}|$) in (1) is limited to $1.15 \cdot 0.5 \cdot V_{\text{dc}}$ for a sine pulsewidth modulation (SPWM) with third harmonic injection [19].
2) *PCS current limit:* The peak value of the converter current ($|i_{\text{cdq}}|$) in (1) is constrained by the peak value of the PCS current ($I_{\text{base}} \cdot \sqrt{2}$). In this context, I_{base} is the nominal rms current value of the PCS.

As the focus of this article is on reactive power provision from BESS-STATCOM, it is now understood that the reactive power is dependent on the fundamental magnitudes of the variables v_{cdq} and v_{sdq}. The value of v_{cdq} in a single-stage BESS-STATCOM depends on the chosen PWM technique, MI, and battery pack voltage v_{bat}. Meanwhile, v_{sdq} on the LV side represents the grid voltage scaled by the turns ratio of the LFT.

Combining all the presented mathematical analysis and algorithms detailed in [20], a power capability curve for both active and reactive power is generated for the BESS-STATCOM, as shown in Fig. 2. The parameters used for this curve are summarized in Table I. The battery pack selected is Li-ion-based and designed to deliver 5 MW for 15 min. The maximum voltage on the dc link for the designed BESS-STATCOM is 1100 V, determined by the open circuit voltage of the battery pack. In Fig. 2, the black and green curves illustrate the PQ capability of the BESS-STATCOM under grid voltages of 1.0 and 0.9 pu, respectively. So, the lower the grid voltage or the higher the dc link voltage, the higher the BESS-STATCOM's reactive power generation capability. For a fixed dc link voltage, Q_{max} at $V_{\text{s}} = 1.0$ pu is 4.17 MVar or 0.83 pu. This means that, if the designed BESS-STATCOM is commanded to support the grid voltage by generating reactive power, the maximum it can generate is 4.17 MVar at $V_{\text{s}} = 1.0$ pu with active power reference set to zero. Whereas Q_{max} at $V_{\text{s}} = 0.9$ pu is 4.49 MVar or 0.89 pu. In most situations, reactive power support service from BESS-STATCOM is expected only when the grid voltage drops to less than 1.0 pu. Therefore, this article focuses on analyzing

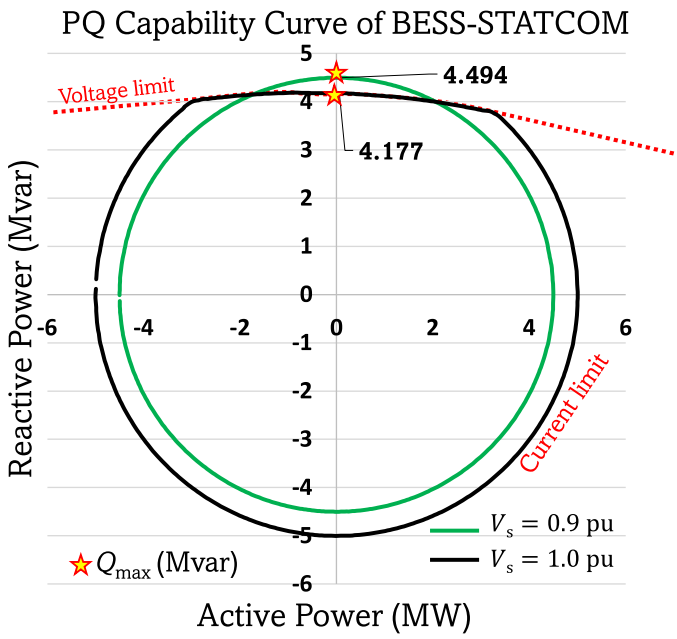

Fig. 2. Active reactive power capability curves of BESS-STATCOM constrained by voltage and current limits.

TABLE I
DESIGN PARAMETERS OF BESS-STATCOM WITH A SINGLE-STAGE PCS

Parameter	Symbol	Value	Per unit
Apparent power base	S_{base}	5 MVA	1.0 pu
Voltage base ac	V_{base}	600 V	1.0 pu
Current base ac	I_{base}	4811 A	1.0 pu
Frequency base ac	f_{base}	50 Hz	1.0 pu
Voltage dc	V_{dc}	1100 V	
Current dc	I_{dc}	4545 A	
Transformer ratio		13.8 kV / 600 V	
Short-circuit inductance	L_{LFT}	18.3 µH	0.08 pu
Short-circuit resistance	R_{LFT}	0.360 mΩ	0.005 pu
Main reactor inductance	L_{f}	67.4 µH	0.293 pu
Main reactor resistance	R_{f}	0.720 mΩ	0.01 pu
Shunt capacitance	C_{f}	2.4 mF	0.055 pu
LCL resonance	f_{res}	850 Hz	
dc capacitance	C_{dc}	20 mF	
Switching frequency	f_{sw}	3000 Hz	

the maximum reactive power generation (Q_{max}) only at $V_{\text{s}} = 0.9$ pu. This sets the basis for the subsequent sections.

B. Impact of Battery Pack Dynamics on Power Capability Curves of BESS-STATCOM

For the discussed BESS-STATCOM, a 5 MW for 15 min battery pack is designed and integrated using a series-parallel combination of many Kokam SLPB120216216 Lithium-ion batteries cells (NMC Chemistry). From the cell datasheet, charging and discharging characteristics against the depth of discharge (DoD) are obtained. Using these characteristics, the charge and discharge resistances of the battery are estimated and saved as lookup tables to be used in the battery model [21]. Thus,

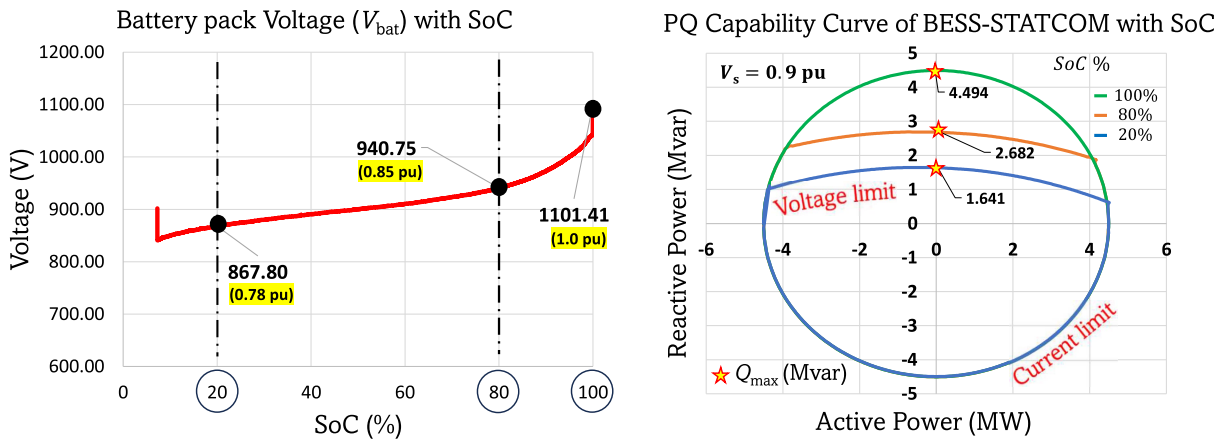

Fig. 3. (a) Battery pack voltage variation with SoC and (b) corresponding capability curve.

the terminal voltage of the battery pack during charging and discharging can be accurately predicted. Also, it is convenient to establish a relationship between the SoC and the battery pack's terminal voltage or the dc link voltage of the PCS. For validating the model, the battery pack is set to discharge 5 MW (1.0 pu) of active power for 900 s (15 min) in simulation, and the variation in battery pack terminal voltage with SoC is shown in Fig. 3(a). The dc link voltage of PCS varies between 0.855 pu for SoC = 80% and 0.788 pu for SoC = 20% , i.e., for a base voltage of 1100 V, i.e., dc-link voltage varies between 940 and 867 V as highlighted in Fig. 3(a).

SoC = 80% and SoC = 20% are marked in black (dashed) in Fig. 3(a) showing the limits of operation, as most of the battery management systems (BMS) ensure the SoC is regulated within these limits by controlled charging and discharging operations for enhancing the lifetime of the battery pack [22]. That implies that the theoretical capability curve in Fig. 2 drawn with an assumption of constant dc link voltage is not valid during the operation of BESS-STATCOM and thus, the dynamic calculation of capability curves is essential. This observation is critical, and to capture the sensitivity of capability curves with battery pack's SoC, three capability curves at SoC = 100% , SoC = 80% , and SoC = 20% are computed and shown as green, orange, and blue curves, respectively, in Fig. 3(b). For grid voltage $V_s = 0.9$ pu, Q_{max} at SoC 80% is around 2.68 MVar (0.53 pu) captured by the orange curve, which is 40% lower than Q_{max} at SoC 100% , i.e., 4.49 MVar (0.89 pu). For the worst case discharge situation, i.e., when BESS is at SoC 20% , Q_{max} is as low as 1.64 MVar (0.32 pu), which is 63% lower than Q_{max} at SoC 100% . This reduction in reactive power capability is not desirable, and thus, a BESS-STATCOM is typically oversized. This article tackles this problem by proposing a reactive power boost control strategy (RBCS), which is discussed in the following section.

C. Verification of Operational Boundaries of BESS-STATCOM

To validate the theoretical figures (see Figs. 2 and 3), a simulation of the BESS-STATCOM in grid-following mode is performed. The outer control loops are designed to regulate the reference powers. The simulation results in Fig. 5(a) show that at 1.0 pu grid voltage, when Q_{pcs_ref} is set to 4.17 MVar and P_{pcs_ref} to zero, the measured Q_{pcs} and P_{pcs} track the reference values. As seen in Fig. 2, at Q_{max} of 4.17 MVar, the voltage limit is reached, which is also confirmed in Fig. 5(b) where the MI saturates at 1.0 pu, while the PCS current (I_c) still has margin. In contrast, at $V_s = 0.9$ pu, Q_{max} increases to 4.49 MVar (0.89 pu), limited by the PCS's current limit. Results in Fig. 5(c) shows that when Q_{pcs_ref} is set to 4.49 MVar and P_{pcs_ref} to zero, the measured powers Q_{pcs} and P_{pcs} tracks the reference accurately. As shown in Fig. 5(d), the PCS's current (I_c) reaches its limit of 1.0 pu, while the MI still has some margin.

Fig. 3 is straightforward to validate through simulation. By varying the dc link voltage proportional to three SoC levels (100% , 80% , and 20%), as shown in Fig. 3(a), BESS-STATCOM is set to generate maximum reactive power, as illustrated in Fig. 3(b). The simulation results in Fig. 6(a) confirms that the maximum reactive power generated by the BESS-STATCOM is 4.49 MVar at SoC = 100% , 2.68 MVar at SoC = 80% , and 1.64 MVar at SoC = 20% , closely matching the theoretical analysis. The accuracy of the current and voltage limitations shown in Fig. 3(b) is further confirmed in Fig. 6(b), which displays the grid voltage, MI, and BESS-PCS converter current in pu. At $V_s = 0.9$ pu, the system is current-limited at SoC = 100% and $Q_{pcs} = 4.49$ MVar, while at SoC = 80% ($Q_{pcs} = 2.68$ MVar) and SoC = 20% ($Q_{pcs} = 1.64$ MVar), it is voltage-limited, validating the analysis.

III. Proposed Reactive Power Boost Strategy

For a given grid voltage, the reactive power capability of a BESS-STATCOM system depends on the maximum voltage on the ac side of its converter, which is determined by the converter's dc link voltage and its maximum allowed MI (e.g., to avoid overmodulation). When a battery is connected directly to the converter's dc link without a dc–dc converter, changes in the battery's SoC directly affect the maximum ac voltage and the reactive power capabilities of the converter. Indeed, at lower SoC, the battery voltage is reduced which limits the converter's ac side voltage and reduces its reactive power capability. In these conditions, the proposed algorithm disconnects

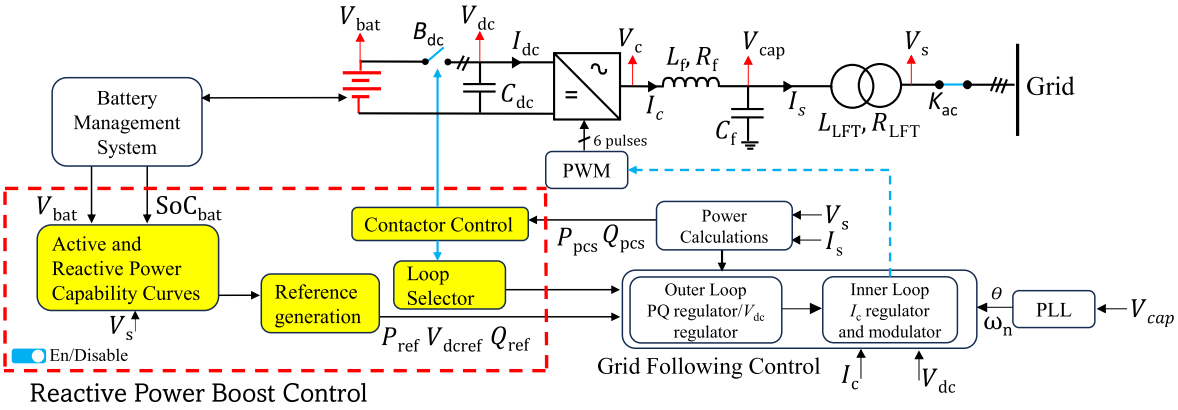

Fig. 4. Block diagram of BESS-STATCOM control with proposed RBCS.

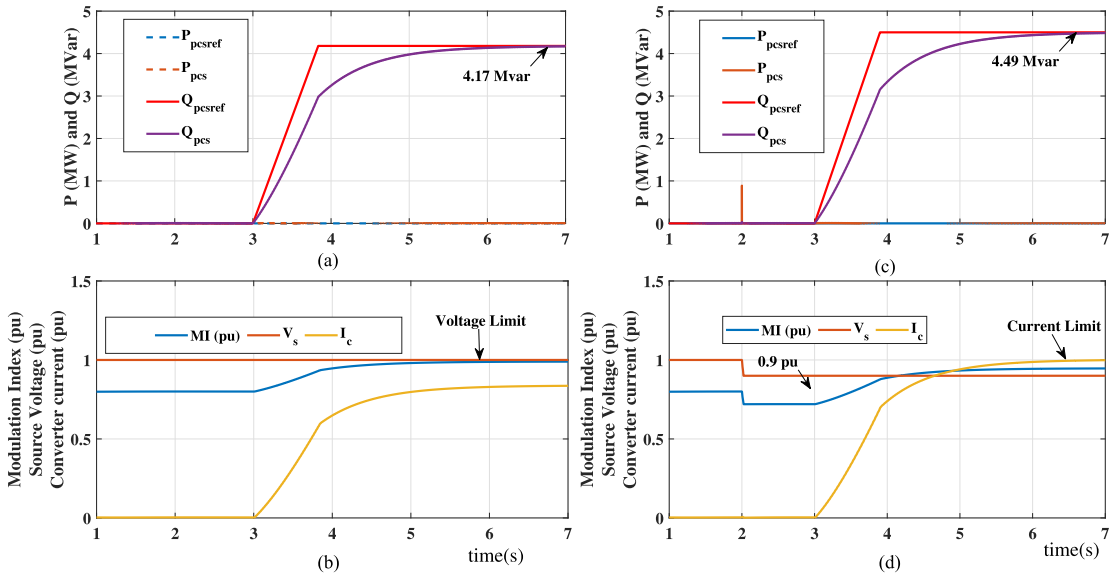

Fig. 5. Simulation results at $V_{dc} = 1100$ V. (a) Power reference and measured powers. (b) Grid voltage, PCS MI, and current at $V_s = 1.0$ pu. (c) Reference and measured powers. (d) Grid voltage, PCS MI, and current at $V_s = 0.9$ pu.

the battery effectively decoupling the dc link voltage from the SoC and charges the dc link capacitor to its rated voltage. This allows to increase the ac side voltage enabling the converter to provide a reactive power boost equivalent to what would be achieved with a fully charged battery. When the battery's SoC is low the BESS-STATCOM's PQ capability curve shifts to align with that of a fully charged battery (100% SoC). Although no active power flow is provided, the proposed method is still justified, as the battery would not be able to support active power at lower SoCs even if it remained connected.

The proposed strategy's control structure is shown in Fig. 4. This strategy relies on two key. 1) The BESS-STATCOM is connected to the battery pack through a dc contactor, and the PCS control can digitally control its status. 2) There is a real-time exchange of measured voltage and SoC of the battery pack from the BMS to the PCS control. While both voltage and SoC are important to monitor, the reactive power capability of the PCS is primarily dependent on the voltage, making it a necessary measurement, whereas SoC, while desirable, is secondary in this context. The SoC information is crucial mainly for indicating when active power services can no longer be delivered due to a discharged condition. This information justifies the transition to an "only reactive power boost" service by disconnecting the battery when necessary. The proposed strategy is highlighted inside a red dashed area with yellow blocks added to the low-bandwidth outer loop of a PCS cascaded control system. The entire sequence of the strategy is captured in the flow chart in Fig. 8. In this case, the PCS control is utilizing grid-following control. As reactive power boost can be a necessary service, for example, for a heavy motor starting or transformer energizing on the grid, a software enabler can request additional reactive power from the BESS-STATCOM, to be triggered only when the grid voltage falls below a specific limit and either the current or voltage limit of the PCS is reached. Before enabling the proposed strategy, active and reactive capability curves are continuously computed dynamically using inputs V_{bat}, SoC, and V_s.

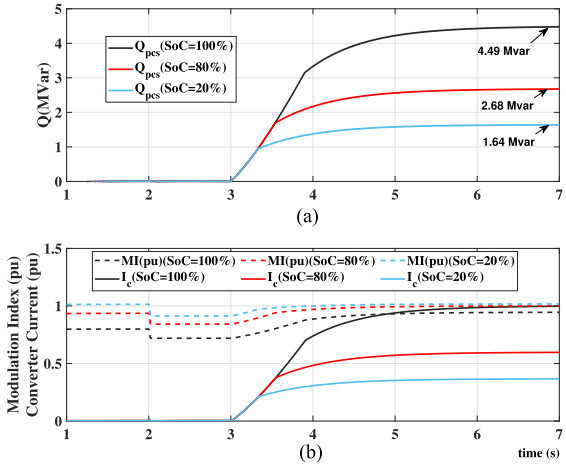

Fig. 6. Simulation results showing operational limits and boundaries from the theoretical curve in Fig. 3. (a) Reactive power of BESS-STATCOM (MVar). (b) Grid voltage, PCS MI, and current (pu) at $V_s = 0.9$ pu for SoC levels of 100% , 80% , and 20% .

When the RBCS is enabled, the outer loops in the PCS control, which are responsible for active and reactive power regulation, are first handled. Their references are set to zero regardless of the state and magnitude of their measured powers. Then, there is a checkpoint to evaluate if the measured active power or dc link current is zero. Once this check is passed, the contactor control block opens the contactor B_{dc} at almost zero dc current. Once the contactor is opened and confirmed, the outer loop selector block switches from active power regulation to V_{dc} regulation of the dc link capacitor (C_{dc}). The capacitor voltage is regulated to the nominal voltage of the battery open circuit voltage by the active power loop. This will increase the reactive power capability of the BESS-STATCOM, as if the battery pack was fully charged. Of course, the reactive power loop will remain unchanged with or without the battery pack connected to the capacitor voltage. In the latter case, only the converter's power losses are drawn from the grid. For the considered system, and its capability curve seen in Fig. 3(b), the BESS-STATCOM capability is expected to shift from the blue curve (worst case when SoC is 20%) to the green curve, giving a boost in reactive power ≈ 2.7 times. Even in the best case when the SoC is at 80% (orange curve), a reactive power boost of ≈ 1.7 times is achieved.

When RBCS is disabled, the reference power of the reactive power loop is set to zero. The V_{dc} reference for the active power loop is set to the measured battery pack terminal voltage. Then, the contactor control block closes the contactor B_{dc} without any inrush current from either the converter or the battery side. This is followed by the outer loop selector block switching back to active power regulation from V_{dc} regulation of the dc link capacitor and continuing its original intended service (referred as normal mode). In Fig. 7, a phasor diagram illustrates how the proposed strategy boosts the reactive power of the BESS-STATCOM system. The diagram shows the grid voltage (V_{s}), the maximum voltage drop across the transformer and filter inductances, the maximum PCS current (I_{c20}, I_{c80}, I_{c100}), and the maximum PCS voltage (V_{c20}, V_{c80}, V_{c100}) at SoC levels of 20% , 80% , and 100% , respectively. When the RBCS is disabled and the battery bank is connected to the PCS, the SoC level of the battery affects the reactive power capability of the BESS-STATCOM. At a low SoC of 20% , the maximum reactive power is constrained by the PCS voltage (V_{c20}), as shown in Fig. 7(a). Although the PCS current (I_{c20}) is below its maximum, the reactive power (Q_{pcs}) from the BESS-STATCOM is limited ($Q_{\text{pcs100}} \gg Q_{\text{pcs80}} \gg Q_{\text{pcs20}}$). In contrast, when the RBCS is enabled and the SoC is low, with a request for reactive power, the dc link capacitor of the PCS is charged to the rated voltage. This allows the PCS to utilize its rated voltage V_{c100}, corresponding to the fully charged battery (SoC = 100%), thereby generating the maximum reactive power Q_{pcs100} at the peak PCS current, as shown in Fig. 7(b). Thus, a reactive power boost is achieved, independent of the battery's SoC level.

IV. Simulation Results and Analysis

This section provides simulation results using MATLAB Simulink to control a BESS-STATCOM, whose design parameters, inspired by an industrial converter [23], are given in Table I. The first point of interest is to prove the theoretical capability curves captured in Fig. 3(b) for the worst case battery SoC being 20% . Then, the proposed algorithm (shown in Figs. 4 and 8) is implemented, and a reactive power boost is achieved. Also, this section explicitly highlights the importance of transitioning between normal mode and reactive power boost mode, through two separate subsections.

A. Normal Mode to Q_{boost} Mode

Simulation results are shown in Fig. 9, capturing the sequence of events for BESS-STATCOM transitioning from normal to boost mode using the proposed RBCS strategy. The initial conditions of operation are 1) battery SoC = 20% ; and 2) active power (P_{pcs}) = 1 MW. The black solid line in Fig. 9(d) captures the LV grid voltage (V_{s}) at the point of common coupling (PCC). At t = 4 s, a low grid voltage of 09 pu is sensed, and BESS-STATCOM, which is originally discharging active power, reacts to the low voltage event and, in response, ramps up the reactive power. The reactive power reference is set to 1.5 MVar closest to the maximum capability at battery pack SoC = 20% , as seen from the red solid line in Fig. 9(b). The measured reactive power (Q_{pcs}) tracks the set reference as desired, seen as a purple solid line in Fig. 9(b). The checkpoint that the converter has reached the maximum reactive power can be better understood by looking at the MI, which is shown as a pink dashed line in Fig. 9(d). The MI is saturated to 1, signifying that the converter reached the voltage limit, although there is enough margin with the converter current (I_{c}) (as seen from the solid blue line in Fig. 9(d). Due to this, the LV grid voltage (V_{s}) at the PCC has improved only to 0.95 pu.

At t = 9 s, RBCS is enabled, initiating the transition from normal to boost mode, as seen from the solid blue line in Fig. 9(a). When the RBCS is enabled, active and reactive regulators set their references to zero, and the measured powers track them accurately, as seen in Fig. 9(b). The battery pack current (I_{bat}), which is a function of P_{pcs}, also drops to zero, [solid green line in Fig. 9(d)]. Once the zero battery pack current is ensured, the

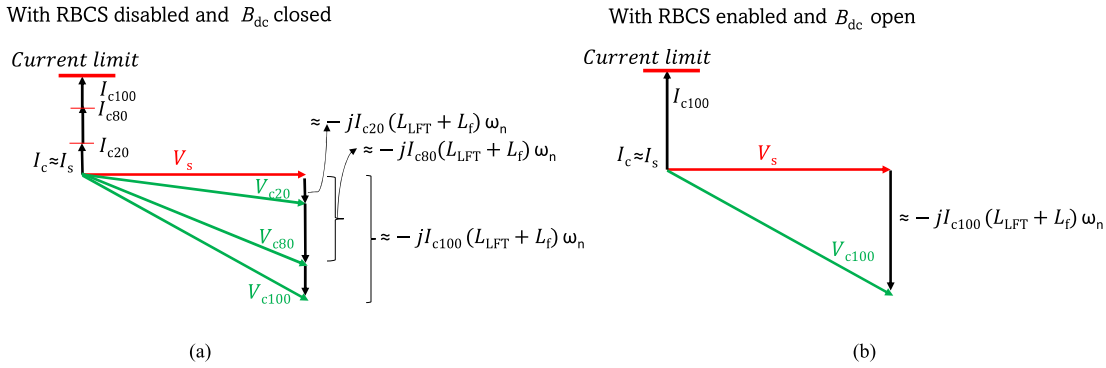

Fig. 7. Phasor diagrams of BESS-STATCOM's reactive power (a) with RBCS disabled and B_{dc} closed, (b) with RBCS enabled and B_{dc} open.

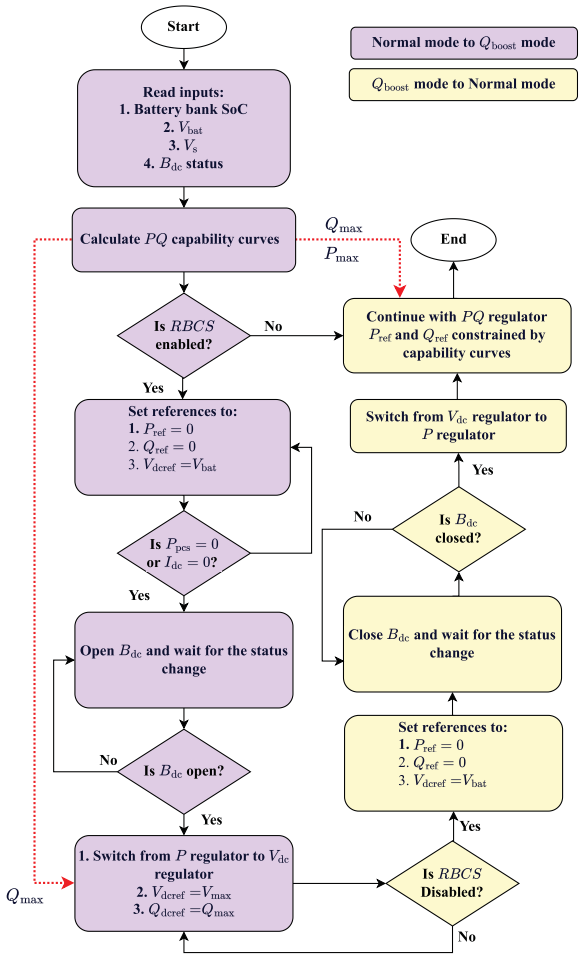

Fig. 8. Flowchart of RBCS.

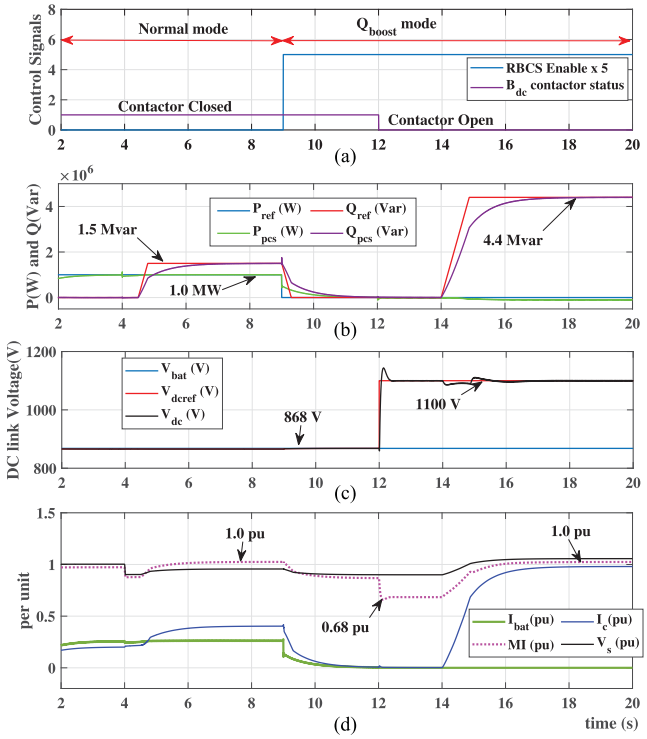

Fig. 9. Simulation results transitioning to Q_{boost} mode with RBCS for a BESS-STATCOM. (a) RBCS activation and B_{dc} contactor status. (b) Reference and measured PCS power. (c) Battery pack and V_{dc} capacitor voltages. (d) Grid voltage, PCS MI, and current (per unit).

contactor B_{dc} is opened. One of the outer loops in the control switches from active power regulation to dc capacitor voltage regulation at t = 12 s. The capacitor dc reference voltage (V_{dcref}) is set to 1100 V (V_{max}) seen as a solid red line in Fig. 9(c). This is the maximum dc voltage that the capacitor is designed to handle when the battery pack SoC is 100% . The measured capacitor voltage (V_{dc}) tracks the reference voltage by charging from the grid, as shown by the solid black line in Fig. 9(c). While the capacitor voltage regulation is achieved, the MI reaches 0.68 pu, creating a significant margin from the voltage limit seen in Fig. 9(d). At $t = 14$ s, the reference reactive power is set to $Q_{max} = 4.4$ MVar, which is the maximum reactive power that BESS-STATCOM can deliver with rated capacitor voltage. The measured reactive power tracks the set reference achieving the reactive power boost as seen in Fig. 9(b). Thus, the transition from normal to boost mode is achieved efficiently, validating the proposed control strategy. It can be seen that V_s at the PCC has improved to 1.0 pu whereas the MI is saturated to 1.0 pu reaching the voltage limit. All the references of regulators are set in a ramp fashion. This is because grid-scale BESS-STATCOMs are typically of high-power capacities, and their utilization is usually

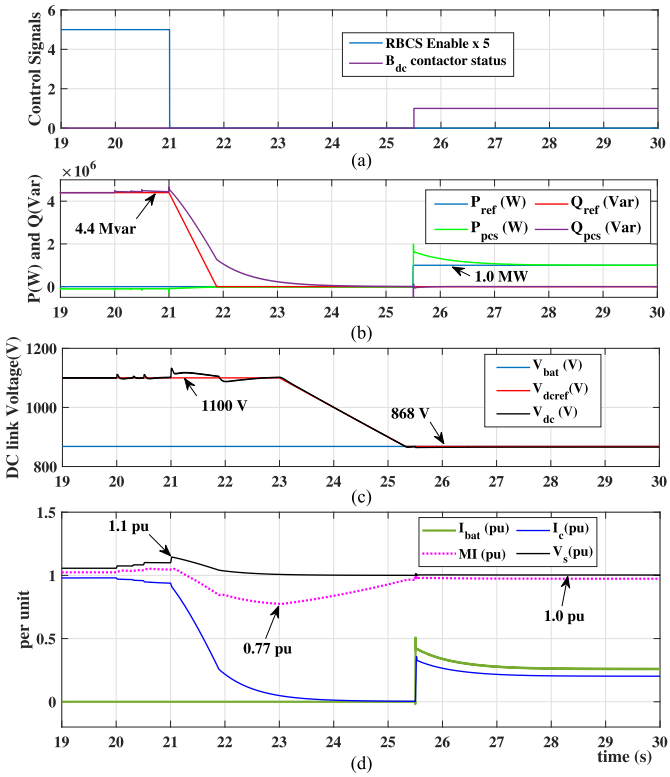

Fig. 10. Simulation results transitioning from Q_{boost} mode to normal mode with RBCS for a BESS-STATCOM. (a) RBCS activation and B_{dc} contactor status. (b) Reference and measured PCS power. (c) Battery pack and V_{dc} capacitor voltages. (d) Grid voltage, PCS MI, and current (per unit).

regulated by standards, limiting the rate of rise in powers to few MW/s or MVar/s.

B. Q_{boost} Mode to Normal Mode

Fig. 10 shows simulation results capturing the sequence of events for BESS-STATCOM transitioning from boost mode to normal mode of operation. This transition begins when the sensed grid voltage (V_{s}) reaches 1.1 pu seen as a black solid line in Fig. 10(d) at $t = 21$s. The proposed RBCS is disabled, initiating the transition from boost to normal mode seen as the solid blue line in Fig. 10(a).

The moment RBCS is disabled, the reactive power regulator sets its reference to zero, and the measured reactive power (Q_{pcs}) tracks the reference accurately, as seen in Fig. 10(b). As a result, the grid voltage reduces close to 1.0 pu in Fig. 10(d). Once the measured reactive power is close to zero, the dc capacitor reference voltage (V_{dcref}) is set to V_{bat} as seen from the solid red line in Fig. 10(c). This is a crucial step to avoid inrush capacitor currents while reclosing the PCS to the battery pack. The measured capacitor voltage tracks the reference voltage by discharging to the grid, which is seen as a solid black line in Fig. 10(c). This sequence of manipulating the reactive power regulator loop first, followed by the dc capacitor voltage regulator, is essential to limit the MI below 1.0 pu. This can be observed in Fig. 10(d). With reactive power tracking to zero and reduced MI, and then by reducing the dc capacitor voltage, the MI is increased back to 1.0 pu. Once the dc capacitor voltage reaches V_{bat}, the contactor B_{dc} closes and connects the PCS to the battery pack. The moment B_{dc} is closed, the active power regulator reference is set to 1 MW, which was the initial condition in normal mode before enabling the RBCS control strategy. The measured active power tracks the set reference as seen in Fig. 10(b). The battery pack current (I_{bat}) and the PCS current (I_{c}) increase proportionally with grid active power as seen in Fig. 10(d). Thus, the transition from boost to normal mode is achieved.

TABLE II
DESIGN PARAMETERS OF SCALED DOWN BESS-STATCOM UTILIZED FOR EXPERIMENTAL TEST BENCH

Parameter	Symbol	Value	Per unit
Apparent power base	S_{base}	32.5 kVA	1.0 pu
Voltage base ac	V_{base}	260 V	1.0 pu
Current base ac	I_{base}	72 A	1.0 pu
Frequency base ac	f_{base}	50 Hz	1.0 pu
Voltage dc	V_{dc}	650 V	
Current dc	I_{dc}	50 A	
Transformer ratio		400 V / 400 V	
Short-circuit inductance	L_{LFT}	316 µH	0.031 pu
Short-circuit resistance	R_{LFT}	49.4 mΩ	0.015 pu
Main reactor inductance	L_{f}	500 µH	0.049 pu
Main reactor resistance	R_{f}	32 mΩ	0.010 pu
Shunt capacitance	C_{f}	50 µF	0.050 pu
LCL resonance	f_{res}	1.61 kHz	
dc capacitance	C_{dc}	14 mF	
Switching frequency	f_{sw}	7 kHz	

V. EXPERIMENTAL RESULTS

The proposed algorithm is validated on a scaled-down BESS at the National Smart Grid Laboratory in Trondheim, Norway. The single-line diagram of the test bed is shown in Fig. 11 and comprises the following.

1) Power amplifier CSU (Compiso System unit) 200 from Egston: This CSU is rated for 200 kVA and has six outputs at 5000 Hz bandwidth, which can create a controllable dc and ac voltage/current source. Two controllable voltage sources (ac and dc) are emulated for this experiment. The ac voltage source (0–400 V) emulates the grid (V_{s}), while the dc source (0–700 V) emulates the battery pack voltage (V_{bat}).
2) A 1:1 delta-wye LFT for galvanic isolation is connected to the emulated grid V_{s}.
3) A three-phase ac contactor with shorted terminals is used as a dc contactor. It is controlled manually with a switch and is powered by a single-phase 230 V electrical outlet.
4) A 260 V, 32.5 kVA, 2-level voltage source converter with an *LC* filter (which, combined with the LFT, forms an *LCL* filter) is used as the PCS. The PCS is connected to the LFT secondary winding on the ac side and a dc contactor on the dc side. The scaled-down PCS's design parameters utilized in the experiment are tabulated in Table II. This test bed supports efficient bidirectional power conversion (which can be interpreted as charging/discharging of BESS via

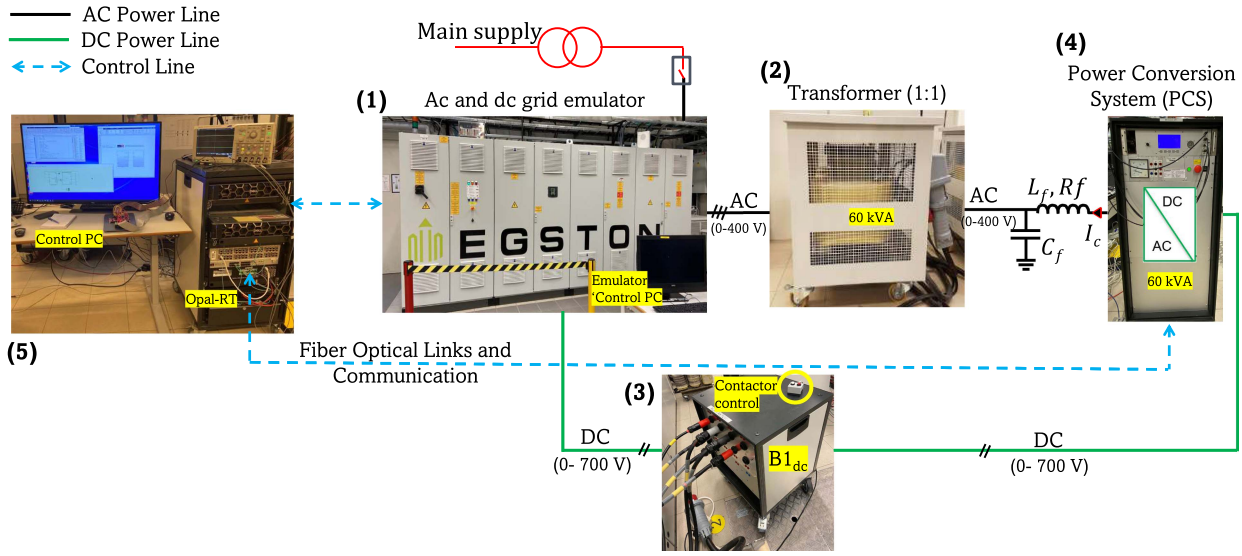

Fig. 11. Experimental test bench of BESS-STATCOM to validate the proposed RBCS strategy.

PCS) because the flown power during experiments from input mains is only the losses resulting from power conversion.

5) A real-time simulator (OPAL-RT OP4520) with RT-Lab software sets the references for the power amplifier and controls the PCS. A grid following control (GFL) of the PCS included with the RBCS strategy is implemented through Simulink model running at a step time of 50 μs. Experimental results are monitored and captured in real-time at 1 ms resolution.

A. *Normal Mode to Q_{boost} Mode*

The experimental results depicted in Fig. 12 illustrate the scaled-down BESS-STATCOM's transition from normal mode to Q_{boost} mode using the proposed RBCS strategy. The initial conditions for experimental validation are observable from t = 0 up to 0.15 s, and the results of the RBCS control procedure follow. The contactor B_{dc} is initially closed, as shown in Fig. 12(a). The battery pack, emulated by the power amplifier, is discharging active power (P_{pcs}) of 10 kW, causing its terminal voltage (V_{bat}) to drop to 485 V (0.74 pu) from 650 V (1.0 pu at SoC = 100%) as shown in Fig. 12(b) and (c) Neglecting the voltage drop across the contactor, V_{dc} and V_{bat} are the same. The voltage V_{s} at the secondary side of the transformer, initially measured as 245 V (0.94 pu), is only improved to 251 V (0.96 pu) when BESS-STATCOM is generating a reactive power (Q_{pcs}) of 12.5 kVar as shown in Fig. 12(b) and (e). At this operating point, the PCS generates the maximum reactive power possible by reaching a maximum MI of 0.95, maintaining sufficient margins for PWM dead time and transient conditions within converter control illustrated in Fig. 12(e).

The experimental results for the transition from normal to Q_{boost} mode are observable from t = 0.15 s to 3 s. At t = 0.15 s, the proposed RBCS control strategy is enabled, shown in [see Fig. 12(a)]. Instantaneously, both outer loop regulators (active and reactive power) set their references to zero, and the measured powers track them accurately in Fig. 12(b). The battery pack current (I_{bat}), a function of the PCS active power, also drops to zero, as seen in Fig. 12(d). Once the zero battery pack current is ensured, the contactor B_{dc} opens at 0.9 s as seen in Fig. 12(a). The dc capacitance (C_{dc}) isolated from battery pack discharges naturally via the shunt-connected discharge resistance from 485 to 440 V shown in [see Fig. 12(c)]. The battery pack voltage (V_{bat}) remains at 485 V, as it is disconnected. At t = 2.15 s, the active power outer loop in the PCS control switches from active power regulation to capacitor voltage regulation. The dc capacitance-voltage regulator sets the reference ((V_{dcref}) to 650 V, which is the maximum battery pack voltage at SoC 100% . The dc capacitor voltage (V_{dc}) tracks V_{dcref} instantly by charging from the grid in Fig. 12(c). This can be observed as negative P_{pcs} transient in Fig. 12(b). While the capacitor voltage regulation is achieved, the MI is observed to reach 0.63 in Fig. 12(e), thus relieving the converter from voltage limit and making it possible to provide a maximum reactive power of 32 kVar in Fig. 12(b) reaching the PCS current limit of 102 A peak before the voltage limit. As a result, the grid voltage (V_{s}) has improved to 260 V (1.0 pu), fully utilizing the reactive power boost. Accordingly, it is shown that the proposed strategy increases the reactive power capability to approximately 2.6 times (12.5–32 kVar) for the same BESS at the discharged condition.

B. *Q_{boost} Mode to Normal Mode*

Fig. 13 shows experimental results of the scaled down BESS-STATCOM transitioning from Q_{boost} to normal mode with the proposed RBCS strategy. In the time interval between t = 6.8 and 7.10 s, the following initial conditions were observed. At t = 7.10 s, the contactor B_{dc} was open, as depicted in Fig. 13(a), showing the disconnection of the emulated battery pack. The dc

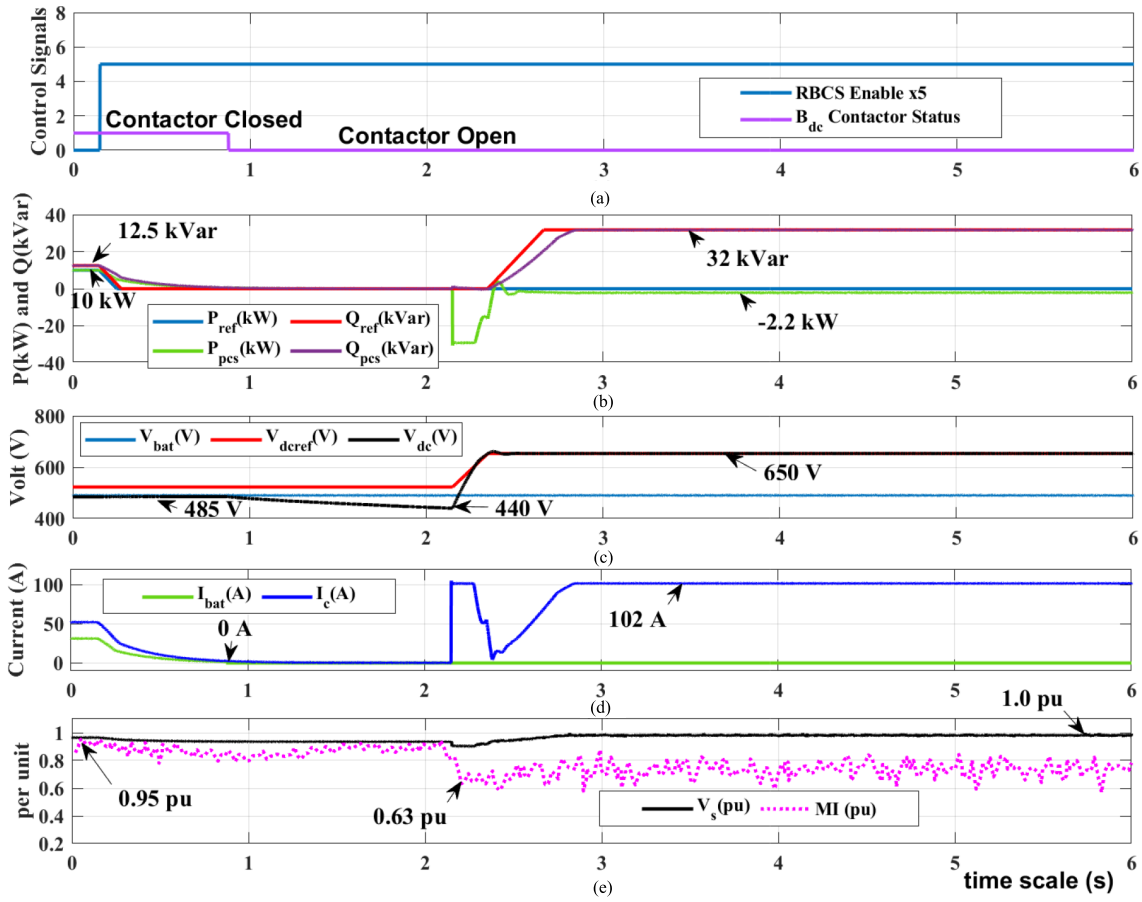

Fig. 12. Experimental results transitioning to Q_{boost} mode with RBCS for a BESS-STATCOM. (a) RBCS activation and B_{dc} contactor status. (b) Reference and measured PCS power. (c) Battery pack and V_{dc} capacitor voltages. (d) Battery pack and PCS currents. (e) Grid voltage (LV side) and PCS MI (per unit).

capacitance voltage (V_{dc}) was measured at 650 V, as illustrated in Fig. 13(c). An active power (P_{pcs}) of -2.2 kW was drawn from the grid, while the BESS-STATCOM in Q_{boost} mode generated a reactive power (Q_{pcs}) of 32 kVar. Furthermore, the voltage (V_{s}) at the secondary side of the transformer improved to 261 V (1.0 pu), as observed in Fig. 13(e). At this operational state, the MI of BESS PCS was measured at 0.65 pu, as depicted in Fig. 13(e).

The experimental results for the transition from Q_{boost} to normal mode are observable from t = 7.10 s up to 9 s. At t = 7.10 s, the proposed RBCS control strategy is disabled, as seen in Fig. 13(a). Instantaneously, the outer loop regulator associated with reactive power sets its reference to zero, and the measured power tracks the reference accurately in Fig. 13(b). The PCS current (I_{c}), a function of PCS active and reactive power, also drops to zero, as seen in Fig. 13(d). After the reactive power reference reaches zero, the outer loop regulator associated with dc capacitor voltage (V_{dc}) sets its reference value close to the disconnected battery pack voltage (V_{bat}). The measured dc capacitor voltage (V_{dc}) tracks the reference of 485 V accurately as shown in Fig. 13(c). At t = 7.75 s, the contactor B_{dc} is closed [see Fig. 13(a)] without inrush currents in I_{bat} or I_{c}, shown in Fig. 13(d), highlighting the advantage of the proposed RBCS strategy. This is possible because the dc capacitor voltage (V_{dc}) and battery pack voltage (V_{bat}) are ensured to be of the same value before the closure of the contactor. At t = 8.5 s, both outer loop regulators (active and reactive power) set their references to initial conditions for returning to normal mode, i.e., an active power (P_{pcs}) of 10 kW and reactive power (Q_{pcs}) of 12.5 kVar, and the measured powers track them accurately in Fig. 13(b). This concludes an efficient transition from Q_{boost} to normal mode. It can be noted that the MI has reached its maximum value of 0.95 pu, the same as the initial condition before enabling the RBCS.

It is worth highlighting that a close match between simulation and experimental results is seen. A slight deviation in regulator performances during transition is due to the differences in time constants of power circuit components and controller bandwidths of full-scale 5 MVA PCS when compared to scaled-down 32.5 kVA laboratory PCS. The controller gains of the current regulators from the scaled down PCS are significantly faster than the gains of full-scale converter considered in the simulation.

VI. Comparative Analysis - Simulation and Experimental

In this section, comparative simulations and experimental results are presented to demonstrate the effectiveness of the proposed method. Fig. 14 shows the simulation results of the BESS-STATCOM both with and without the RBCS strategy. The initial conditions include delivering 1 MW of active power (P_{pcs})

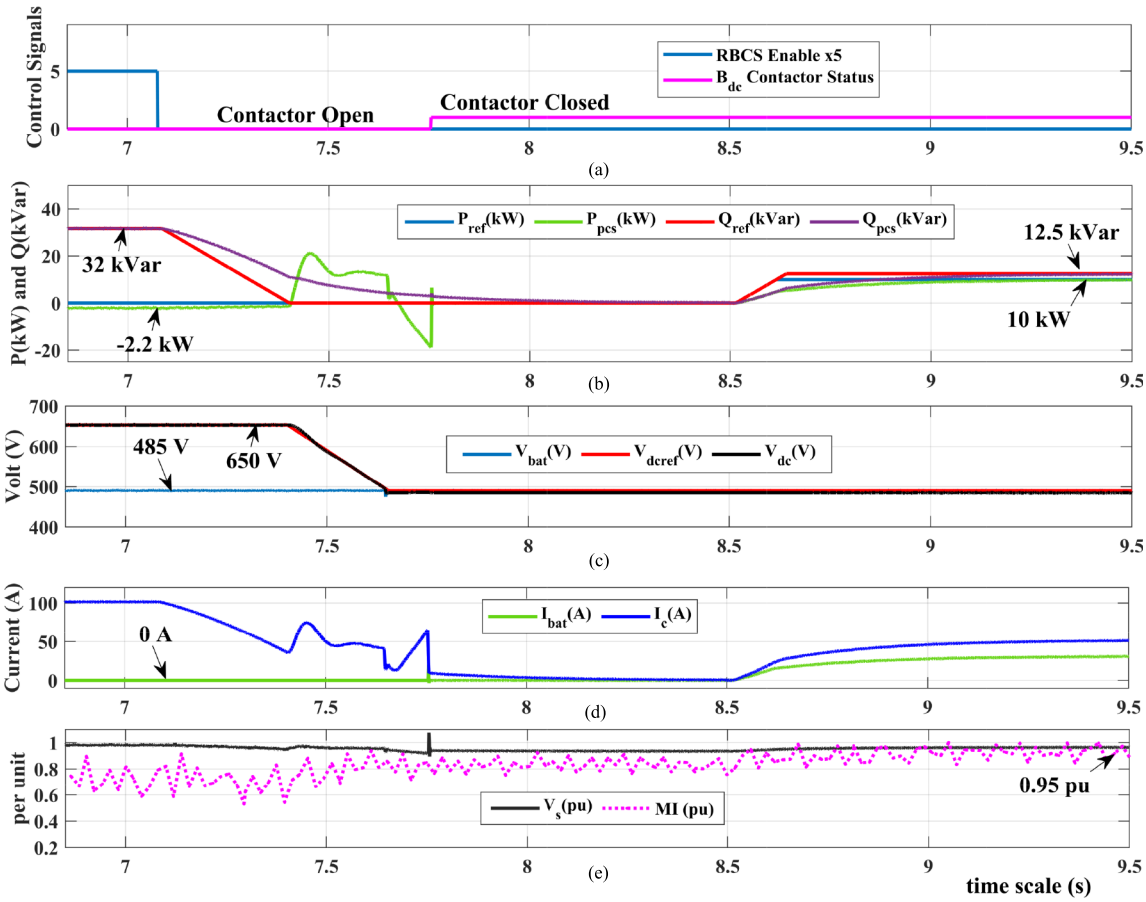

Fig. 13. Experimental results depicting the transition from Q_{boost} mode to normal mode with RBCS for a BESS-STATCOM. (a) RBCS activation and B_{dc} contactor status. (b) Reference and measured PCS power. (c) Battery pack and V_{dc} capacitor voltages. (d) Battery pack and PCS currents. (e) Grid voltage (LV side) and PCS MI (per unit).

and the battery SoC at 20% ($V_{\text{dc}} = V_{\text{bat}} = 868$ V). At this point, reactive power support is requested when the grid voltage is at $V_{\text{s}} = 0.9$ pu. Without the method, BESS-STATCOM generates a maximum reactive power (Q_{pcs}) of 1.5 Mvar [see Fig. 14(a)], nearing the voltage limit as indicated by the MI [see Fig. 14(c)]. With the method, the battery disconnects, and the dc link voltage is regulated to 1100 V [see Fig. 14(b)], boosting Q_{pcs} to 4.4 Mvar—a threefold increase. Similarly, Fig. 15 shows experimental results for a scaled-down BESS-STATCOM. When delivering 10 kW (P_{pcs}) and with the battery SoC at 20% ($V_{\text{dc}} = V_{\text{bat}} = 485$ V), reactive power support is requested at $V_{\text{s}} = 0.9$ pu. Without the method, Q_{pcs} reaches 12.5 kVAR [see Fig. 15(a)], with the MI saturating at 1.0 pu [see Fig. 15(c)]. With the method, the battery disconnects, and the dc link voltage charges to 650 V, increasing Q_{pcs} to 32 kVAR—approximately 2.56 times higher [see Fig. 15(a)].

VII. Feasibility for Multilevel BESS-STATCOMs

In this section, a three-level (3L) neutral-point-clamped (NPC) converter shown in Fig. 16, is considered as the PCS to evaluate the feasibility of the proposed strategy for multilevel converters-based BESS-STATCOMs. A detailed switching model of the 3L-NPC topology is used to capture all switching-frequency-related transients. In 3L-NPC, regulating the dc-link voltage involves controlling the total voltage (V_{dc}) and balancing the top and bottom capacitor voltages (V_{dctop}, V_{dcbot}) after the breaker (B_{dc}) disconnects the battery. This is achieved using a dc voltage regulator and a capacitor balancing controller [24], which introduces a common-mode voltage proportional to the imbalance by adjusting the MI. Thus, capacitors can charge or discharge via common-mode current through their midpoint, remaining unaffected by battery connection or disconnection.

For the considered PCS whose parameters are derived from [25], simulation results are shown in Fig. 17, capturing the sequence of events for a BESS-STATCOM transitioning from normal to boost mode using the proposed RBCS strategy. The initial operating conditions are 1) battery SoC = 20% ; and 2) active power (P_{pcs}) = 0.1 pu. The black solid line in Fig. 17(c) captures the grid voltage (V_{s}) at the PCC. At t = 2 s, a low grid voltage of 0.9 pu is sensed, and the BESS-STATCOM, which is originally discharging active power, reacts to the low voltage event and ramps up the reactive power in response. The reactive power reference is set to 0.3 pu closest to the maximum capability at battery pack SoC = 20% , as seen from the red solid line in Fig. 17(a). The measured reactive power (Q_{pcs}) tracks the set reference as desired, seen as a purple solid line in

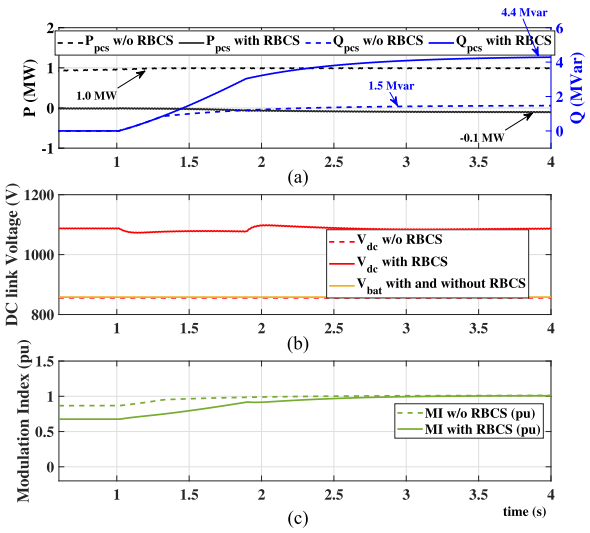

Fig. 14. Comparative simulation results for BESS-STATCOM with and without RBCS. (a) Reference and measured PCS power. (c) Battery pack and V_{dc} capacitor voltages. (d) Modulation index (pu).

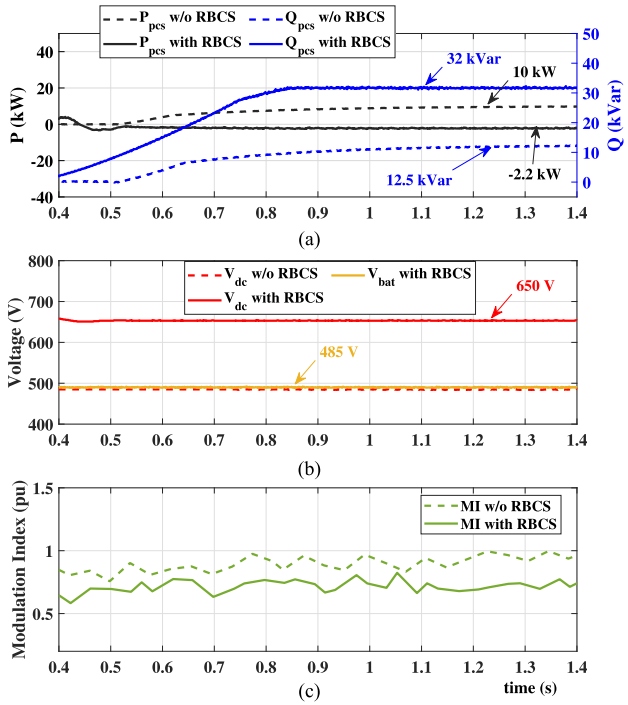

Fig. 15. Comparative experimental results for BESS-STATCOM with and without RBCS. (a) Reference and measured PCS power. (c) Battery pack and V_{dc} capacitor voltages. (d) Modulation index (pu).

Fig. 17(a). The point at which the converter reaches its maximum reactive power can be better understood by examining the MI, represented by the pink dashed line in Fig. 17(c). The MI is saturated to ≈ 1.0 pu, signifying that the converter reached the voltage limit although there is enough margin with the converter current (I_c) [solid blue line in Fig. 17(c)]. Due to this, the grid voltage (V_s) at the PCC has improved only to 0.95 pu.

At t = 4 s, RBCS is enabled, initiating the transition from normal to boost mode, as seen from the dashed blue line in

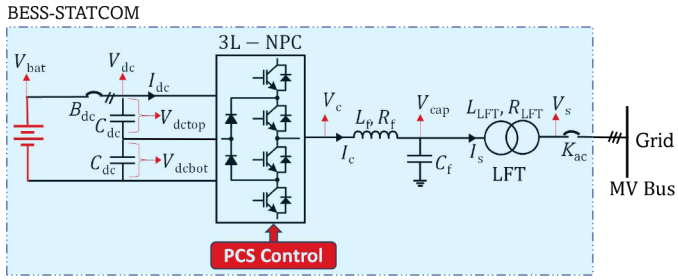

Fig. 16. Single line diagram of 3L-NPC-based BESS-STATCOM.

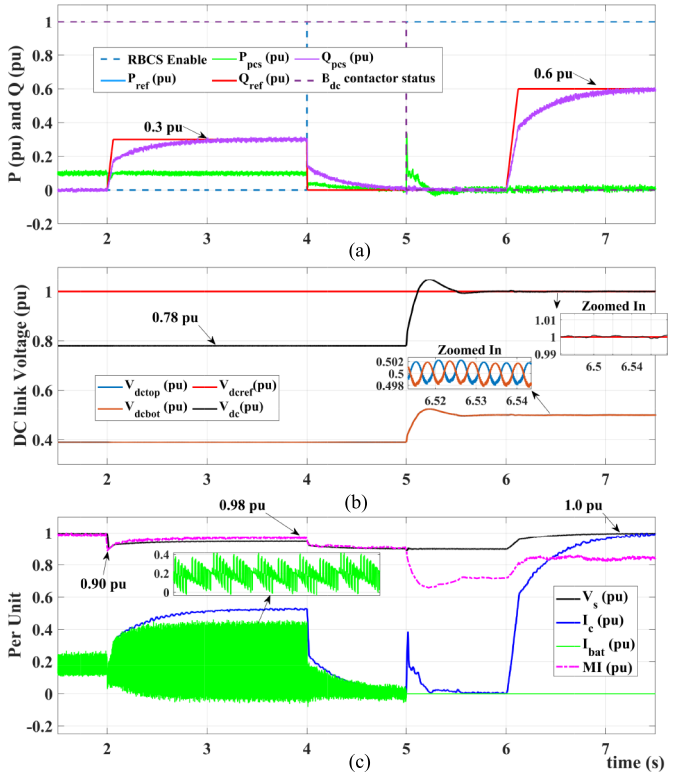

Fig. 17. Simulation results transitioning from Q_{boost} mode to normal mode with RBCS for a 3L-NPC-based BESS-STATCOM. (a) RBCS activation, B_{dc} contactor status, reference, and measured PCS power. (b) Reference and V_{dc} top, bottom, and total capacitor voltages. (c) Grid voltage, PCS MI, and current (per unit).

Fig. 17(a). When the RBCS is enabled, active and reactive regulators set their references to zero, and the measured powers track them accurately, as seen in Fig. 17(a). The battery pack current (I_{bat}), which is a function of P_{pcs}, also drops to zero, [solid green line in Fig. 17(c), with a zoomed figure showing switching ripple].

Once the zero average battery pack current is ensured, the contactor B_{dc} is opened. The control outer loop switches from active power regulation to dc-link voltage regulation at t = 5 s. The capacitor dc reference voltage (V_{dcref}) is set to 1.0 pu (V_{max}) seen as a solid red line in Fig. 17(b). This is the maximum dc voltage that the capacitor is designed to handle when the battery pack SoC is 100% . The measured capacitor voltage (V_{dc}) tracks the reference voltage by charging from the grid, as shown by

the solid black line in Fig. 17(b). Moreover, the two capacitor voltage V_{dctop} and V_{dcbot} are well balanced by the balancing algorithm. While the capacitor voltage regulation is achieved, the MI reaches 0.66 pu, creating a significant margin from the voltage limit seen in Fig. 17(c). At $t = 6$ s, the reactive power reference is set to $Q_{\text{max}} = 0.6$ pu (maximum at rated capacitor voltage). The measured reactive power tracks the set reference achieving the reactive power boost as seen in Fig. 17(a). Thus, the proposed RBCS strategy enhances the reactive power on 3L-NPC-based BESS-STATCOM (nearly doubling it) at lower SoC's by seamlessly disconnecting the battery and charging the dc link capacitors without disrupting capacitor voltage balance. The strategy integrates smoothly into existing converter controls and is versatile enough to adapt to various multilevel topologies (e.g., active NPC, flying capacitor, modular multilevel converters) when they are directly connected to the dc link without an intermediate dc–dc converter.

VIII. Conclusion

This article presents a novel control strategy for boosting the reactive power capability from BESS-STATCOM, which consists of a single-stage PCS connected to an electrical grid. The proposed strategy involves a seamless transition from normal to Q_{boost} mode and vice versa, effectively increasing the system's reactive power capability by almost threefold. The reactive power boost effectively raises the BESS-STATCOM's reactive power capability to match that of a BESS-STATCOM with a fully charged battery pack. In addition, the transition for the proposed strategy has been proven to occur at zero battery current, eliminating the need for an expensive dc circuit breaker. Simulations for a 5 MVA BESS-STATCOM (2-level and 3-level PCS) and experimental validation on a 32.5 kVA 2-level PCS confirm the effectiveness of the proposed strategy. Though this article does not quantify cost and space savings, the findings suggest significant potential benefits, especially for space-constrained applications requiring an oversized BESS-STATCOM for reactive power support.

References

[1] S. Sharma et al., "A comprehensive review on STATCOM: Paradigm of modeling, control, stability, optimal location, integration, application, and installation," *IEEE Access*, vol. 12, pp. 2701–2729, 2024.

[2] T. Engelbrecht et al., "STATCOM technology evolution for tomorrow's grid: E-STATCOM, STATCOM with supercapacitor-based active power capability," *IEEE Power Energy Mag.*, vol. 21, no. 2, pp. 30–39, Mar./Apr. 2023.

[3] F. Zhao et al., "Energy-storage enhanced STATCOMs for wind power plants," *IEEE Power Electron. Mag.*, vol. 10, no. 2, pp. 34–39, Jun. 2023.

[4] G. G. Farivar et al., "Grid-connected energy storage systems: State-of-the-art and emerging technologies," *Proc. IEEE*, vol. 111, no. 4, pp. 397–420, Apr. 2023.

[5] S. Ponnaluri, G. Linhofer, J. Steinke, and P. Steimer, "Comparison of single and two stage topologies for interface of BESS or fuel cell system using the abb standard power electronics building blocks," in *Proc. Eur. Conf. Power Electron. Appl.*, 2005, Art. no. 9.

[6] G. Wang et al., "A review of power electronics for grid connection of utility-scale battery energy storage systems," *IEEE Trans. Sustain. Energy*, vol. 7, no. 4, pp. 1778–1790, Oct. 2016.

[7] L. S. Xavier, C. V. De Sousa, H. A. Pereira, and V. F. Mendes, "Design and performance comparisons of power converters for battery energy storage systems," *Int. J. Circuit Theory Appl.*, vol. 51, no. 7, pp. 3146–3166, 2023.

[8] A. Kanchanaharuthai, V. Chankong, and K. A. Loparo, "Transient stability and voltage regulation in multimachine power systems vis-à-vis statcom and battery energy storage," *IEEE Trans. Power Syst.*, vol. 30, no. 5, pp. 2404–2416, Sep. 2015.

[9] I. Serban and C. Marinescu, "Control strategy of three-phase battery energy storage systems for frequency support in microgrids and with uninterrupted supply of local loads," *IEEE Trans. Power Electron.*, vol. 29, no. 9, pp. 5010–5020, Sep. 2014.

[10] J.-T. Gao, C.-H. Shih, C.-W. Lee, and K.-Y. Lo, "An active and reactive power controller for battery energy storage system in microgrids," *IEEE Access*, vol. 10, pp. 10490–10499, 2022.

[11] R. K. Varma, M. Ahmadi, and C. Arpino, "Novel control of battery energy storage system (BESS) as statcom (BESS-STATCOM) for stabilization of a critical motor," in *Proc. IEEE Can. Conf. Elect. Comput. Eng.*, 2023, pp. 261–267.

[12] M. G. Dozein, O. Gomis-Bellmunt, and P. Mancarella, "Simultaneous provision of dynamic active and reactive power response from utility-scale battery energy storage systems in weak grids," *IEEE Trans. Power Syst.*, vol. 36, no. 6, pp. 5548–5557, Nov. 2021.

[13] D. J. Ryan, R. Razzaghi, H. D. Torresan, A. Karimi, and B. Bahrani, "Grid-supporting battery energy storage systems in islanded microgrids: A data-driven control approach," *IEEE Trans. Sustain. Energy*, vol. 12, no. 2, pp. 834–846, Apr. 2021.

[14] A. Zecchino, Z. Yuan, F. Sossan, R. Cherkaoui, and M. Paolone, "Optimal provision of concurrent primary frequency and local voltage control from a bess considering variable capability curves: Modelling and experimental assessment," *Elect. Power Syst. Res.*, vol. 190, 2021, Art. no. 106643.

[15] Z. Yuan, A. Zecchino, R. Cherkaoui, and M. Paolone, "Real-time control of battery energy storage systems to provide ancillary services considering voltage-dependent capability of DC-AC converters," *IEEE Trans. Smart Grid*, vol. 12, no. 5, pp. 4164–4175, Sep. 2021.

[16] H. Xie, L. Angquist, and H.-P. Nee, "Design study of a converter interface interconnecting energy storage with the DC link of a StatCom," *IEEE Trans. Power Del.*, vol. 26, no. 4, pp. 2676–2686, Oct. 2011.

[17] L. S. Araujo, N. T. D. Fernandes, D. I. Brandao, and B. J. C. Filho, "Smartbattery: An active-battery solution for energy storage system," in *Proc. IEEE 15th Braz. Power Electron. Conf., 5th IEEE Southern Power Electron. Conf.*, 2019, pp. 1–6.

[18] C. J. O'Rourke, M. M. Qasim, M. R. Overlin, and J. L. Kirtley, "A geometric interpretation of reference frames and transformations: Dq0, clarke, and park," *IEEE Trans. Energy Convers.*, vol. 34, no. 4, pp. 2070–2083, Dec. 2019.

[19] S. N. Vukosavic, *Grid-side converters control and design: Interfacing between the AC grid and renewable power sources*, 1st ed., Ser. Power Electronics and Power Systems. Cham, Switzerland: Springer, 2018.

[20] H. S. Das, S. Li, B. Lu, J. Wang, S. Rahman, and X. Fu, "Exploring dynamic P-Q capability and abnormal operations of inverter-based resources," *IEEE Trans. Emerg. Sel. Topics Power Electron.*, vol. 12, no. 2, pp. 1608–1618, Apr. 2024.

[21] J. V. Barreras, E. Schaltz, S. J. Andreasen, and T. Minko, "Datasheet-based modeling of li-ion batteries," in *Proc. IEEE Veh. Power Propulsion Conf.*, 2012, pp. 830–835.

[22] G. Rancilio, A. Rossi, C. Di Profio, M. Alborghetti, A. Galliani, and M. Merlo, "Grid-scale BESS for ancillary services provision: Soc restoration strategies," *Appl. Sci.*, vol. 10, no. 12, 2020, Art. no. 4121. [Online]. Available: https://www.mdpi.com/2076-3417/10/12/4121

[23] "PS1000 690Vac and LVACS880 power conversion system technical catalogue," Hitachi Energy, Zurich, Switzerland, Datasheet 4CAE000825, 2022. [Online]. Available: PS1000-690Vac-Data-sheet-A4-4CAE000825

[24] N. Celanovic and D. Boroyevich, "A comprehensive study of neutral-point voltage balancing problem in three-level neutral-point-clamped voltage source PWM inverters," *IEEE Trans. Power Electron.*, vol. 15, no. 2, pp. 242–249, Mar. 2000.

[25] J. Banda, S. Chapaloglou, and E. Tedeschi, "MV multi-functional retrofit converter for enhanced power quality on O&G platforms," in *Proc. IEEE 13th Int. Symp. Power Electron. Distrib. Gener. Syst.*, 2022, pp. 1–6.